A novel motif in calcimembrin/C16orf74 dictates multimeric dephosphorylation by calcineurin

*Devin A. Bradburn[1], *Joana C. Reis[2,3], Haribabu Arthanari[2,3], Martha S. Cyert[1#]

1. Department of Biology, Stanford University, Stanford, CA 94305, USA
2. Department of Cancer Biology, Dana-Farber Cancer Institute, Boston, Massachusetts, USA.
3. Department of Biological Chemistry and Molecular Pharmacology, Harvard Medical School, Boston, Massachusetts, USA.

**Contributed equally to this work*
#Corresponding author: E-mail address: mcyert@stanford.edu

Abstract

Calcineurin (CN), the only Ca^{2+}-calmodulin activated protein phosphatase, dephosphorylates substrates within membrane-associated Ca^{2+} microdomains. CN binds to substrates and regulators via short linear motifs (SLIMs), PxIxIT and LxVP. PxIxIT binding to CN is Ca^{2+} independent and affects its distribution, while LxVP associates only with the active enzyme and promotes catalysis. 31 human proteins contain one or more composite 'LxVPxIxIT' motifs, whose functional properties have not been examined. Here we report studies of calcimembrin/C16orf74 (CLMB), a largely uncharacterized protein containing a composite motif that binds and directs CN to membranes. We demonstrate that CLMB associates with membranes via N-myristoylation and dynamic S-acylation and is dephosphorylated by CN on Thr44. The LxVP and PxIxIT portions of the CLMB composite sequence, together with Thr44 phosphorylation, confer high affinity PxIxIT-mediated binding to CN (KD~8.9 nM) via an extended, ^{33}LxVPxIxITxx(p)T^{44} sequence. This binding promotes CLMB-based targeting of CN to membranes, but also protects Thr44 from dephosphorylation. Thus, we propose that CN dephosphorylates CLMB in multimeric complexes, where one CLMB molecule recruits CN to membranes via PxIxIT binding, allowing others to engage through their LxVP motif for dephosphorylation. This unique mechanism makes dephosphorylation sensitive to CLMB:CN ratios and is supported by *in vivo* and *in vitro* analyses. CLMB overexpression is associated with poor prognoses for several cancers, suggesting that it promotes oncogenesis by shaping CN signaling.

Key words: Calcium, phosphatase, calcineurin, S-acylation, signaling, SLiM

Introduction

Calcium (Ca^{2+}) ions are spatially and temporally controlled in cells to regulate a wide array of biological processes. Ca^{2+} signaling occurs within membrane-associated microdomains that contain both effector proteins and their substrates. Thus, subcellular localization of calcineurin (CN), the only Ca^{2+}-calmodulin (CaM) regulated serine/threonine protein phosphatase, dictates its signaling specificity[1]. CN interacts with partners via two short linear motifs (SLiMs), referred to as LxVP and PxIxIT, that cooperate to promote dephosphorylation. PxIxIT binding occurs independent of Ca^{2+}-signals and anchors CN to substrates, which increases their local concentration, and to regulators, such as scaffold protein A kinase anchoring protein 5 (AKAP5)[2], which directs CN to localized signaling domains. LxVP binding helps to orient substrates for dephosphorylation at a separate catalytic site, marked by a Zn^{2+} and Fe^{2+} ion[3]. The LxVP docking site on CN is accessible only after activation by Ca^{2+}/CaM binding and is blocked by the autoinhibitory C-terminal tail of CN as well as the immunosuppressant drugs, Cyclosporin A and FK506[4, 5]. Systematic identification of these motifs has significantly expanded our knowledge of CN substrates and functions[6-9] and identified 31 human proteins that contain a novel CN binding motif. This motif, referred to as a composite motif, contains both LxVP and PxIxIT in a single sequence with a shared proline (LxVPxIxIT)[9]. Both parts of composite motifs can bind their cognate site on CN, but are unlikely to engage these docking surfaces, which are ~60 angstroms apart, simultaneously. Thus, how or if these motifs function to promote dephosphorylation is unclear. Here we examine the function of a composite motif in C16orf74, a short, unstructured, and largely uncharacterized protein that is associated with poor outcomes in

melanoma, pancreatic and head and neck cancer[10, 11]. Because C16orf74 binds to and recruits CN to membranes[10], we have named it calcimembrin (CLMB).

In this work we show that CLMB associates with membranes via two lipid modifications, N-myristoylation and S-acylation. S-acylation, the only protein lipidation that is reversible, regulates many aspects of signaling at membranes [12]. In addition to CLMB, S-acylation modulates CN activity through at least two additional mechanisms: S-acylation regulates subcellular localization of the AKAP5 scaffold in neurons to control long-term synaptic potentiation[13]. Also, the naturally occurring CN isoform, CNAβ1, contains an S-acylated C-terminus, which allows this enzyme to dephosphorylate membrane-associated substrates such as the phosphatidyl-inositol-4-kinase IIIα (PI4KIIIIα) complex[14].

Previous studies showed that CLMB binding to CN requires phosphorylation of Thr44 and is disrupted when the central 'PxIxIT' sequence is deleted, which also compromises the 'LxVP' portion of the motif [10, 15]. Our studies carefully dissect the composite motif to elucidate how both the PxIxIT and LxVP portions of this sequence contribute to CN-CLMB interactions. We demonstrate that CN dephosphorylates CLMB at Thr44, which requires the 'LxVP' sequence. In addition, detailed binding analyses show that the composite motif confers extremely strong PxIxIT-mediated binding to CN, which is strengthened by flanking LxVP and phospho-Thr44 features.

Furthermore, our work establishes that the composite LxVPxIxITxx(p)T motif confers unique signaling properties to CLMB. Using in-cell assays, together with *in vitro* dephosphorylation, we show that CLMB dephosphorylation is strongly influenced by the CLMB:CN ratio, supporting a model in which CN dephosphorylates CLMB in a multimeric complex. We propose that one CLMB molecule provides a high affinity PxIxIT motif and recruits CN to membranes via regulated S-acylation, where it dephosphorylates other CLMB molecules via LxVP-mediated interactions causing an overall decrease in CLMB affinity for CN. In summary, this work establishes that composite motifs not only mediate dephosphorylation but can also shape CN signaling through novel mechanisms.

Results

Calcimembrin is myristoylated and S-acylated. CLMB is a small, disordered protein with no predicted transmembrane domains (Figure 1A) that associates with membranes[10]. We investigated whether protein lipidation might be responsible for this localization. C16orf74 contains an N-terminal glycine (G2), a common site for N-myristoylation, the co-translational addition of a 14-carbon lipid which often contributes to membrane association in combination with other lipid modifications[16]. These include S-acylation, the reversible addition of a fatty acid, usually a 16-carbon palmitate, to the sidechain of cysteine residues[12]. CLMB has two cysteines near in its N-terminus, Cys7 and Cys14, one of which, Cys7, is predicted to be palmitoylated[17]. These cysteines have previously been implicated in CLMB dimer formation via disulfide bonds[18]. To determine if CLMB is lipidated, we incubated HEK293 Flp-In T-REx cells inducibly expressing wildtype CLMB-FLAG ($CLMB4_{WT}$) with YnMyr and 17-ODYA, alkyne-containing analogs of myristate and palmitate respectively[19]. Following immunoprecipitation, analog incorporation was detected via addition of biotin using CLICK-chemistry followed by visualization with streptavidin (Figure 1B). $CLMB_{WT}$ incorporated YnMyr and 17-ODYA, indicating the presence of both lipids. To determine sites of lipidation, we mutated both C7 and C14 to serine ($CLMB_{C7,14S}$), which eliminated 17-ODYA incorporation while maintaining YnMyr incorporation. By contrast, neither lipid modification was detected for $CLMB_{G2A}$ (Figure 1B). We

noted low expression of these mutants, suggesting that lipidation enhances protein stability. For this reason, a proteasome inhibitor (MG132) was included in all assays examining CLMB lipidation mutants.

To determine if CLMB-FLAG is dually S-acylated at Cys7 and Cys14, we used an acyl-PEG exchange assay in which S-acylated groups are exchanged for a PEGylated molecule that increases protein mass by 5 kDa for each S-acylated residue[20] (Figure 1C). $CLMB_{WT}$ displayed two slower migrating bands representing singly- and dually S-acylated forms of the protein. $CLMB_{C7S}$ lacked the upper band, while $CLMB_{C7,14S}$ was unmodified, indicating that C7 and C14 of FLAG-$CLMB_{WT}$ are both S-acylated. $CLMB_{G2A}$ also displayed two sites of S-acylation in these analyses, suggesting that the metabolic labeling experiment (1B) was not sufficiently sensitive, given low protein expression, to detect these modifications. Together these findings suggest that CLMB is myristoylated at Gly2 and S-acylated at Cys7 and Cys14.

S-acylation of CLMB is dynamic and mediates membrane association. S-acylation, the only protein lipidation that is reversible, turns over rapidly for some proteins, while others are stably modified[12]. To examine the dynamics of CLMB-FLAG S-acylation we carried out a pair of pulse-chase analyses with two metabolic labels (Figure 1D and 1E). L-AHA, an azide-containing methionine analog detected CLMB-FLAG protein levels, while in parallel, 17-ODYA detected palmitoylation. After a one-hour pulse, analogs were removed for a 30-minute chase with DMSO or Palmostatin B (PalmB), a small molecule pan-inhibitor of depalmitoylases[21], followed by immunopurification of CLMB-FLAG. Quantifying the 17-ODYA to L-AHA ratio showed that CLMB palmitate incorporation increased ~3-fold when depalmitoylation was inhibited (PalmB vs DMSO). Thus, CLMB palmitoylation, which turns over rapidly relative to protein degradation, is dynamic.

To determine if lipidation mediates CLMB membrane recruitment, we utilized detergent assisted subcellular fractionation. While $CLMB_{WT}$ was primarily found in membrane fractions, both $CLMB_{G2A}$ and $CLMB_{C7,14S}$ were predominantly cytosolic (Figure 1F and 1G). Therefore, N-myristoylation and dynamic dual S-acylation of CLMB stabilize the protein and allow it to associate with membranes.

The composite SLIM in CLMB mediates binding to and dephosphorylation by calcineurin. Because CLMB contains an unusual composite LxVPxIxIT motif, LDVPDIIIT, we examined how each part of this sequence might function with respect to CN by generating two mutants, $CLMB_{IxITMut}$ (LDVPD**A**I**AA**) and $CLMB_{LxVMut}$, (**A**D**A**PDIIIT) to disrupt each motif separately without altering the shared proline. To examine binding of these mutants to CN, CLMB-FLAG constructs and GFP-tagged CN (CNA-GFP) were co-transfected into HEK293 cells, with immunoprecipitation of CNA-GFP from these lysates used to assess association with CLMB (Figure 2A and 2B). $CLMB_{WT}$ co-immunoprecipitated with CNA-GFP and this interaction was PxIxIT dependent, as $CLMB_{IxITMut}$ failed to co-purify. This is consistent with demonstrated roles for PxIxIT motifs mediating stable association with CN[5]. $CLMB_{LxVMut}$ displayed reduced co-purification, indicating that, to a lesser extent, it also contributes to CN binding. Additionally, examining the input samples for these immunoprecipitations, showed that both mutants displayed a second band with decreased electrophoretic mobility, which is also faintly present for $CLMB_{WT}$, although with a smaller change in electrophoretic mobility. These slower migrating forms of CLMB are eliminated upon mutation of threonine 44 to alanine, i.e. in $CLMB_{T44A}$ and $CLMB_{T44A+LxVMut}$, and thus represent CLMB that is phosphorylated at this residue. This

observation suggests that CLMB binds to and is dephosphorylated by CN, and that disrupting either the LxVP or PxIxIT portion of the composite motif prevents dephosphorylation. Finally, we observed that the slower migrating form of both $CLMB_{WT}$ and $CLMB_{LxVMut}$ predominantly co-purified with CN, suggesting, as previously reported, that phosphorylation at T44 enhances binding to CN[10]. Indeed, $CLMB_{T44A}$ displayed reduced binding to CN, which was further reduced by mutating both LxV and T44 ($CLMB_{T44A+LxVMut}$).

The contributions of the PxIxIT, LxVP, and T44 phosphorylation to binding are also reflected in the ability of CLMB to recruit CN to membranes. Immunofluorescence (IF) shows that $CLMB_{WT}$-FLAG recruits CN-GFP to membranes, when co-transfected into MCF7 cells (Figure 2C, 2D). However, CN is largely cytosolic and colocalizes poorly when co-expressed with $CLMB_{IxITMut}$. $CLMB_{LxVMut}$ and $CLMB_{T44A}$ show minor but significant reductions in colocalization with CN, mirroring the trends observed with co-immunoprecipitation experiments.

Dephosphorylation of Thr44 by CN was confirmed *in vitro* using a phosphorylated peptide substrate encoding residues 21-50 of CLMB (Figure 1A and 2 E). In contrast, a peptide encoding the sequence from $CLMB_{LxVMut}$ failed to be dephosphorylated showing that, similar to other CN substrates, the LxVP motif is required for dephosphorylation. Together, these data show that both the LxVP and PxIxIT components of the composite motif are functional, that CLMB is a CN substrate, and indicate that phosphorylation enhances CLMB binding to CN.

Phosphorylation and the LxVP motif enhance PxIxIT binding. Our data show that the LxVP, PxIxIT, and T44 phosphorylation of CLMB are all required for maximal binding to CN, but it is not clear how they do so. To quantitatively assess each component's contribution to binding, we used fluorescence polarization anisotropy (FP) and isothermal titration calorimetry (ITC) to measure binding affinities between CN and CLMB peptides containing the composite SLiM (residues 21-50). This was done using a catalytically dead and truncated CN ($CN_{Trunc+H151Q}$). Truncation removes the autoinhibitory C-terminal region of CNA, allowing CN to bind both LxVP and PxIxIT motifs in the absence of Ca^{2+} and CaM[22]. ITC revealed that phosphorylated $CLMB_{WT}$ ($pCLMB_{WT}$) binds CN at a one-to-one ratio with the highest reported affinity for a CN substrate, (K_D= 8.29 nM), (Figure 3A). To assess the contribution of phosphorylation to CN binding, we compared the binding affinities of $pCLMB_{WT}$ to non-phosphorylated $CLMB_{WT}$ using FP with FITC-labelled peptides. This revealed ~30-fold weaker binding for the non-phosphorylated peptide (K_D = 384.5 nM vs 12.29nM) (Figure 3B), with affinities in good agreement between the ITC and FP analyses (8.29 vs 12.29 nM for $pCLMB_{WT}$). Because the PxIxIT motif was required for CLMB co-immunoprecipitation with CN, this high affinity interaction is likely PxIxIT-mediated. To test this, we used FP to assess the ability of CLMB peptides to compete with PVIVIT, a well characterized PxIxIT peptide[23, 24] for CN binding (Figure 3C). $pCLMB_{WT}$ competed with PVIVIT most effectively, (Figure 3C, 3E) with decreased competition exhibited when the LxV motif was mutated ($pCLMB_{LxVMut}$), or T44 was not phosphorylated ($CLMB_{WT}$). $pCLMB_{IxITMut}$ lacking the PxIxIT motif was unable to displace PVIVIT from CN. A very similar pattern was observed when these experiments were repeated using $pCLMB_{WT}$ peptide in place of PVIVIT (Figure 3D), suggesting that like PVIVIT, $pCLMB_{WT}$ also engages CN primarily through the PxIxIT motif. Altogether, these data show that CLMB binding to the PxIxIT docking groove on CN is enhanced by residues flanking the core PxIxIT, i.e. LxV and pT44, to form an extended LxVPxIxITxxT(p) sequence.

Calcineurin dephosphorylates CLMB by forming multimers. Having demonstrated how different sequence elements in CLMB contribute to PxIxIT-mediated binding to CN, we next investigated how the LxVP and PxIxIT portions of this composite motif cooperate to promote dephosphorylation of pThr44. Unexpectedly, we observed that phosphorylation of $CLMB_{WT}$ *in vivo* was sensitive to levels of CN expression. When $CLMB_{WT}$ was inducibly expressed in HEK293 Flp-In T-REx cells with endogenous levels of CN, the slower migrating phosphorylated form of $CLMB_{WT}$ was not observed but did appear in cells that were transfected with GFP-CNA to increase overall CN levels (Figure 4A, compare first two lanes). We hypothesized that this paradoxical behavior may stem from the unique nature of the LxVPxIxITxxT(p) motif. When phosphorylated CLMB interacts with CN via high affinity PxIxIT binding, pThr44 is not able to access the catalytic site for dephosphorylation. However, a second molecule of CLMB could engage with this CLMB-CN complex via a lower affinity LxVP -mediated interaction and be dephosphorylated. Thus, by increasing the CN:CLMB ratio, CN overexpression promotes non-productive binding of CLMB(pT44) through the PxIxIT motif. This model predicts that dephosphorylation should be rescued by overexpressing additional CLMB to decrease the CN:CLMB ratio. To test this prediction, we transfected CN alone or alongside V5-tagged CLMB constructs into HEK293 Flp-In T-REx cells inducibly expressing CLMB-FLAG. In fact, we did observe that expressing additional $CLMB_{WT}$-V5 reduced levels of phosphorylated $CLMB_{WT}$-FLAG in cells co-expressing GFP-CNA (Figure 4A and B). This ability of additional CLMB to rescue dephosphorylaton was dependent on PxIxIT binding as $CLMB_{IxITMut}$-V5 overexpression had no effect on $CLMB_{WT}$-FLAG phosphorylation. $CLMB_{LxVMut}$-V5 rescued to the same extent at $CLMB_{WT}$-V5, likely due to its intact PxIxIT motif. We repeated these experiments using $CLMB_{IxITMut}$-FLAG, which is partially phosphorylated regardless of CN overexpression. Surprisingly, $CLMB_{IxITMut}$-FLAG was predominantly dephosphorylated when co-expressed with $CLMB_{WT}$-V5 or $CLMB_{LxVMut}$-V5 but not $CLMB_{IxITMut}$-V5 (Figure 4A and B). These data show that the LxVP and PxIxIT components of the CLMB composite motif are both necessary for dephosphorylation, but do not need to be on the same molecule. A single copy of CLMB must have an LxVP to mediate its own dephosphorylation but can utilize the PxIxIT of neighboring copies to recruit CN, promote LxVP binding, and be dephosphorylated.

To determine quantitatively how the ratio of CLMB to CN affects dephosphorylation, we conducted a series of *in vitro* dephosphorylation assays using a fixed CLMB peptide concentration (200nM) with varied CN concentrations (20nM, 100nM and 200nM) (Figure 4C and 4D). For canonical substrates, increasing CN concentration accelerates dephosphorylation until binding is saturated, behavior we observed for $pCLMB_{IxITMut}$, which contains only an LxVP motif (Figure 4E). By contrast, dephosphorylation of $pCLMB_{WT}$ became faster when CN increased from 20nM to 100nM, but showed no further rate enhancement when CN and $pCLMB_{WT}$ were both present at 200nM. Under these conditions, $pCLMB_{IxITMut}$ was dephosphorylated ~3x faster than $pCLMB_{WT}$ (0.362 ± 0.010 min^{-1} vs 0.133 ± 0.002 min^{-1}) These findings are consistent with our model, which predicts that high CN concentrations relative to $pCLMB_{WT}$ slow dephosphorylation by promoting the formation of non-productive PxIxIT-bound CN-CLMB dimers. Together, these data provide evidence for a new mode of CN regulation conferred by the unusual phosphorylated composite motif in CLMB. In addition to activation by Ca^{2+} and CaM, dephosphorylation of this composite motif requires substrate levels to exceed CN, allowing multimers to form.

Discussion

In this study, we show that CLMB, a small, disordered protein and CN substrate, employs several unique biochemical mechanisms to regulate CN signaling. Here we present two models for how CLMB may shape CN activity *in vivo*. Dynamic S-acylation allows CLMB to associate with membranes (Figure 5A, Step 1). Under basal conditions, phosphorylated CLMB binds to inactive CN via its high affinity phosphorylated PxIxIT (Figure 5A, Step 2). In the presence of a Ca^{2+} signal, Ca^{2+} and CaM activate CN and expose the LxVP docking site. If CLMB is in excess relative to CN, this allows a second molecule to bind via the LxVP motif which positions the phospho-Thr44 for dephosphorylation at the active site (Step 3). As the population of CLMB shifts to the non-phosphorylated form, PxIxIT binding affinity decreases. This releases CN, which is now able to engage and dephosphorylate other LxVP and PxIxIT containing substrates at the membrane (Fig 5A, Step 4). Alternatively, active CN-CLMB dimers may directly engage substrates that only contain an LxVP to mediate their dephosphorylation (Figure 5B, step 3). Then, as in 5A step 4, formation of CN-CLMB multimers and subsequent dephosphorylation releases CN from the membrane. Both mechanisms would promote dephosphorylation of membrane localized CN substrates. Our future goals are to identify these substrates and learn more about the local regulation of CN and CLMB concentrations, to fully understand if and how these mechanisms function physiologically.

CLMB S-acylation critically contributes to several features of our proposed model. First, the extent of S-acylation will determine the amount of CN that is positioned at the membrane. Second, by concentrating CLMB, S-acylation facilitates multimer formation which is essential for linking the functions of the LxVP and PxIxIT motifs. Because S-acylation is reversible, this modification can dynamically control the local CN-CLMB ratio. As we showed *in vitro* and *in vivo*, this ratio determines the extent and dynamics of CLMB dephosphorylation which will determine how much CN is available to interact with and regulate other substrates. Thus, identifying which palmitoyl acyltransferases (PATs) and acyl protein thioesterases (APTs) dynamically regulate CLMB membrane association will provide key insights into how S-acylation impacts CN-CLMB signaling *in vivo*. This represents a third context in which S-acylation regulates CN signaling at membranes[13, 14].

Our studies are the first to show how a composite LxVPxIxIT motif, present in at least thirty additional human proteins[9], might function. Using mutations that separate these motifs, we show that the PxIxIT and LxVP sequences within CLMB function identically to all known PxIxIT and LxVP motifs by mediating stable binding and dephosphorylation respectively[5]. However, the upstream Leu and Val residues also enhance PxIxIT binding. Previous studies showed that a hydrophobic residue in the -1 position strengthens PxIxIT binding[25]. Although the -3 position has not been systematically tested, we note that PxIxIT-containing peptides we identified previously using proteomic peptide phage display, are enriched for hydrophobic residues at the -1 and -3 positions[9]. Thus, enhanced PxIxIT affinity may be a common feature of composite motifs. Importantly, we also show that composite motifs confer a new mode of dephosphorylation that requires the formation of multimeric complexes. This may also be a general property of composite LxVPxIxIT motifs, which occur in several ion channels that assemble into higher order complexes, such as CACNA1H[9, 26]. Thus, composite motifs may provide a safety mechanism, to ensure that CN dephosphorylates some proteins only in multimeric forms.

A missing player in our model is the kinase(s) that phosphorylates Thr44 CLMB. Because dephosphorylation decreases affinity, this establishes a negative feedback mechanism by which CN decreases interaction with its own substrate. Thus, potential regulation of the kinase(s) that phosphorylates CLMB may also alter signaling dynamics. Phosphorylation at the +9 position also enhances the affinity of the PxIxIT motif in Cabin1, a CN regulator that like CLMB, contains a PxIxIT followed by "PPTP" [25, 27]. The stress-activated p38 mitogen-activated protein kinase (MAPK) phosphorylates Cabin1 and is predicted to phosphorylate T44 of CLMB[28]. Therefore, future identification of the kinase(s) that phosphorylates CLMB may reveal additional mechanisms that regulate this signaling response.

The major challenge that lies ahead is to identify the molecular targets and physiological functions that are regulated by CN-CLMB. When overexpressed in non-transformed fibroblasts, CN-CLMB increased invasion, and CLMB promotes proliferation and migration of some pancreatic ductal adenocarcinoma (PDAC) derived cell lines[10]. This suggests that CLMB shapes CN signaling to regulate oncogenesis. Indeed high CLMB expression is associated with poor patient outcomes for PDAC, melanoma and head and neck cancer[10, 11]. Mechanisms underlying these activities have not yet been identified, but these cancers may provide good starting points for examining how CLMB modifies CN signaling in a biologically and clinically relevant context.

Materials and Methods

Cell culture and transfection:
Cells were cultured at 37 °C in 5% CO_2. HEK293 Flp-In TReX and MCF7 cell lines were grown in standard media containing Dulbecco's modified eagle's medium (DMEM) with 4.5mg/mL glucose, L-glutamine, and sodium pyruvate (Cytiva SH30243.FS) supplemented with 10% fetal bovine serum (Corning MT35010CV). Transfections were done according to manufacturer instructions. HEK293 cells were transfected using lipofectamine 2000 (Thermo Fisher Scientific 11668019). MCF7 cells were transfected using Transfex ATCC transfection reagent (ATCC ACS-4005).

Stable cell line generation:
On day one, 9.6 x 10^5 HEK293 Flp-In TReX cells were transfected using lipofectamine 2000 with 1.5µg pOG44 and 0. 5µg pcDNA5 FRT TO encoding proteins of interest in a 6 well dish (plasmid # 2801, 2852, 2860, 2861, 2862, 2863, 2864, and 2880). Transfections were done according to manufacturer instructions. On day two, transfected cells were passaged onto 10cm plates. On day three, selection was started using media containing 3µg blasticidin and 200ng/mL hygromycin. Selection media was replaced every 2-3 days until distinct colonies appeared. Colonies were selected using cloning rings and expanded before being stored in liquid nitrogen.

Metabolic labeling to detect CLMB lipidation:
HEK293 Flp-In TReX lines stably expressing $CLMB_{WT}$, $CLMB_{C7,14S}$, or $CLMB_{G2A}$ were induced with 10ng/ml doxycycline for 24 hours and split evenly among three 10cm tissue culture dishes. The following day, cells were rinsed with PBS and incubated in DMEM containing 4.5mg/mL glucose, L-glutamine, sodium pyruvate, 2% FBS, and either 20µM YnMyr (Click Chemistry Tools 1164-5), 30µM 17-ODYA (Cayman Chemical Company 34450-18-5), or vehicle (ethanol and DMSO) overnight. Cells were then co-incubated with 20µM YnMyr, 30µM 17-ODYA, or vehicle and 20µM MG132 (EMD Millipore 474787-10MG) for 4 hours before washed twice in PBS and frozen at -80C. Cells were lysed in 400µL TEA lysis buffer (50mM TEA pH 7.4, 150mM NaCl,

1% triton X-100, and 1mM PMSF) by inverting for 15 minutes at 4°C. Lysates were passed five times through 27-gauge needle, centrifuged at 16,000 x *g* for 15 minutes at 4°C and protein content determined by Pierce BCA protein assay kit (Thermo Fisher Scientific 23225). 25µg total lysate was removed as input and 0.5mg total protein was incubated with pre-washed magnetic M2 anti-FLAG (Sigma-Aldrich M8823-5ML) beads at 4°C for 1.5 hours while inverting. Beads were washed 3X with modified RIPA (50mM TEA pH 7.4, 150mM NaCl, 1% Triton X-100, 0.1% SDS, and 1% sodium deoxycholate) and resuspended in 40ml 1x PBS. 10 ml of 5x click reaction mix (1x PBS, 0.5mM biotin azide, 5mM TCEP, 0.5mM TBTA, 5mM $CuSO_4$) was added and reactions incubated for 1 hour at 24°C, shaking at 550 RPM. Beads were washed 3X in modified RIPA and eluted 2X using 30 ml of 1mg/ml FLAG peptide in modified RIPA buffer. 12 ml of non-reducing 6x SDS sample buffer was added to eluate before heating at 95°C for 2 minutes and analysis by SDS-PAGE. Note that addition of reducing agents to SDS sample buffer results in loss of 17-ODYA signal. Samples were transferred to nitrocellulose membrane and lipidation was detected using fluorophore-tagged streptavidin, and total CLMB with anti-FLAG. Immunoblots were imaged using a Licor Odyssey CLx and quantified with Image Studio software.

Metabolic pulse-chase labeling assay to assess CLMB dynamic palmitoylation
HEK293 Flp-In TReX cells stably expressing $CLMB_{WT}$-FLAG were induced with 10ng/ml doxycycline for 48 hours. Cells were rinsed 2X in PBS and incubated in methionine free DMEM supplemented with 5% charcoal-stripped FBS, 1mM L-glutamate, 1mM sodium pyruvate, 0.4mM cysteine and 10ng/ml doxycycline along with vehicle (ethanol), 30mM 17-ODYA,50mM L-AHA, or 17-ODYA and L-AHA together. After two hours, cells were washed 2X in PBS and either harvested immediately or incubated in standard media supplemented with 10mM palmitic acid and 10ng/ml doxycycline, with or without 10mM palmostatin B (EMD Millipore 178501-5MG). Cells were rinsed in PBS and frozen at -80C. Metabolic labeling was done as described in the previous section with the exception that two rounds of labeling were done. First, Cy5-azide (Click Chemistry Tools AZ118-1) was linked to 17-ODYA. Then, cells were washed and L-AHA was linked to AF-488 (Click Chemistry Tools 1277-1) alkyne before being washed three additional times and eluted using FLAG peptide. Samples were resolved via SDS-PAGE and in-gel fluorescence was read using the GE Amersham Typhoon imaging system. Images were quantified in Image Studio. The proportion of palmitoylated CLMB is calculated as Cy5/A-488 normalized to the no chase control.

Acyl-PEG exchange:
HEK293 Flp-In TReX lines stably expressing $CLMB_{WT}$, $CLMB_{C7S}$, $CLMB_{C7,14S}$, or $CLMB_{G2A}$ were induced with 10ng/ml doxycycline for 48 hours. Cells were rinsed 2X in PBS and stored at -80°C. Cells were lysed in 400ml lysis buffer (50mM TEA pH 7.3, 150mM NaCl, 2.5% SDS, 1mM PMSF, 100 units benzonase) at 37°C for 20 minutes, shaking at 800 RPM. Lysates were passed 10X through a 27-gauge needle, centrifuged at 16,000 x *g* for 5 minutes and protein quantified by BCA. Lysates were adjusted to 2mg/ml and incubated with 10mM TCEP for 30 minutes at room temperature. Cysteines were protected by incubating with 25mM NEM for 2 hours at 40°C, shaking at 800RPM. Protein was precipitated over night with four volumes of acetone at -20°C, centrifuged at 16,000 x *g* for 20 minutes at 4°C and washed 4X in 70% acetone. Acetone was removed, pellets air-dried to remove all traces of acetone and resuspended in 75ml Buffer A (50mM TEA pH 7.3, 150mM NaCl, 4% SDS, 0.2% triton X-100, 4mM EDTA) for 1 hour at 40°C, shaking at 800 RPM. Samples were centrifuged at 16,000 x *g* for 2 minutes, 7ml removed as input, and the remainder split into +cleavage and -cleavage fractions. The +cleavage sample containing 1% SDS was treated with hydroxylamine, final concentration, 750mM for 1 hour at 30°C, rotating end over end. Following methanol-chloroform precipitation (ice cold, final concentrations 42% methanol, 16% chloroform) samples were centrifuged at 16,000 x *g* for 20

minutes at 4ºC, aqueous layer removed, washed 3X with 100% methanol and air dried. Pellets were resuspended as described in Buffer A and incubated in 1mM mPEG-Mal (Methoxypolyethylene glycol maleimide, 5 kDa, 63187 Sigma-Aldrich) for 2 hours at room temp, rotating end over end. Samples were methanol-chloroform precipitated as described, resuspended in Lysis buffer with 1X SDS-PAGE sample buffer, resolved using SDS-PAGE and visualized via immunoblotting with mouse anti-FLAG to detect CLMB-FLAG. Endogenous calnexin was detected using anti-calnexin antibodies. Immunoblots were imaged using a Licor Odyssey CLx and quantified with Image Studio software.

Detergent-assisted subcellular fractionation:
HEK293 Flp-In TReX lines stably expressing $CLMB_{WT}$, $CLMB_{C7,14S}$, or $CLMB_{G2A}$ were induced with 10ng/ml doxycycline for 48 hours and 20µM MG132 (EDM Millipore 474787-10MG) for 4 hours prior to harvesting. Cells were washed 2X in PBS, harvested and immediately lysed in 600ml of Cytoplasm Buffer (10mM HEPES pH6.8, 100mM NaCl, 300mM sucrose, 3mM $MgCl_2$, 5mM EDTA, 1x halt protease inhibitor cocktail (Thermo Fischer scientific 78442)) at 4ºC for 15 minutes. 60 ml of total lysate was removed as input and the remainder centrifuged at 1000 x *g* for 10 min at 4ºC. The supernatant was removed as cytoplasmic fraction and the pellet washed 2X in PBS and resuspended in 600 ml membrane buffer (10mM HEPES pH7.5, 100mM NaCl, 300mM sucrose, 3mM $MgCl_2$, 3mM EDTA, 0.5% Triton X-100, 1x halt protease inhibitor cocktail) for 30 minutes at 4ºC turning end over end. Insoluble material was pelleted by centrifugation at 5000 x *g* for 10 minutes at 4ºC and supernatant removed as membrane fraction. Both fractions were centrifuged at 12,000 x *g* at 4ºC for 10 minutes. Samples were heated in 1X SDS sample buffer at 95ºC for 5 minutes, resolved via SDS-PAGE, immunoblotted and CLMB-FLAG detected using anti-FLAG antibodies; anti-GM130 and anti-α-tubulin were used as membrane and cytosolic markers respectively. Immunoblots were imaged using a Licor Odyssey CLx and quantified with Image Studio software. CLMB in cytosolic and membrane fractions were quantified as $CLMB_{Cyto}/(CLMB_{Cyto}+ CLMB_{Memb})$ and $CLMB_{Mem}/(CLMB_{Cyto} + CLMB_{Memb})$, respectively.

Immunofluorescence, microscopy, and image analysis:
MCF7 cells were co-transfected (as described previously) with equal amounts of pcDNA5 encoding $CLMB_{WT}$, $CLMB_{IxITMut}$, $CLMB_{LxVMut}$, $CLMB_{T44A}$ and pcDNA5 encoding CNA-GFP. The following day cells were plated on poly-lysine coated 12 mm, #1.5H glass coverslips (ThorLabs). On day three, cells were washed in PBS and fixed in 100% methanol for 10 minutes at -20ºC. Coverslips were washed 3X in 1x PBS, blocked (1x PBS, 200mM glycine, 2.5% FBS) for 30 minutes at room temperature, then incubated in primary antibody diluted in blocking buffer for 1 hour before being washed 3X in 1x PBS and incubated for 1 hour in secondary antibody solution. Following three additional washes, coverslips were mounted using Prolong Glass mountant with NucBlue stain. After sitting overnight at room temperature, coverslips were imaged using a Lionheart FX automated widefield microscope with a 20X Plan Fluorite WD 6.6 NP 0.45 objective. For each coverslip, a 7 by 7 grid of non-overlapping images was automatically taken. All images were manually assessed and those with defects (debris, bubbles, out-of-focus, etc.) were filtered out. Images were analyzed using an automated pipeline using CellProfiler[29]. Briefly, cells were identified by their nuclei and all those lacking CLMB-FLAG staining removed. CLMB-FLAG signal was used to define the cell body and all cells containing one or more fully saturated pixels in the CLMB-FLAG or CNA-GFP channels were removed. Pearson's correlation coefficient between CLMB-FLAG and CNA-GFP was determined for each individual cell. >500 cells per condition were analyzed.

GFP-Trap coimmunoprecipitation:

HEK293 cells were co-transfected (as described previously) with pcDNA5 encoding CNA-GFP and pcDNA5 encoding $CLMB_{WT}$, $CLMB_{IxITMut}$, $CLMB_{LxVMut}$, $CLMB_{T44A}$, or $CLMB_{LxVMut+T44A}$. 24 hours post-transfection, cells were washed 2X in PBS and frozen at -80ºC. Cells were lysed in 500ml lysis buffer (50mM Tris pH 7.5, 150mM NaCl, 1% NP-40), aspirated 5X with a 27-gauge needle, centrifuged at 16,000 x *g* for 20 min at 4ºC and protein quantified via BCA. 100mg total protein was removed as input. Lysates were adjusted to 0.5% NP-40 and 500mg of protein incubated with pre-washed magnetic GFP-TRAP beads (ChromoTek gtma-20) for 2 hours at 4ºC, turning end over end. Beads were magnetized, washed 3X and eluted with 50mlof 2x SDS PAGE sample buffer. Samples were resolved via SDS-PAGE and visualized via immunoblotting with anti-flag antibodies to detect CLMB-FLAG and anti-GFP to detect CNA-GFP. Anti-GAPDH was used as a loading control for inputs. Immunoblots were imaged using a Licor Odyssey CLx and CLMB-calcineurin binding was quantified with Image Studio software. Co-purified CLMB was normalized using the following: $(CLMB_{IP}/CLMB_{Input})/GFP\text{-}CNA_{IP}$. Additionally, all values are displayed relative to $CLMB_{WT}$ which is set at 1.

***In vivo* analysis of CLMB phosphorylation status**
HEK293 FLIP-In TreX cells stably expressing $CLMB_{WT}$-FLAG, $CLMB_{IxITMut}$-FLAG, $CLMB_{LxVMut}$-FLAG, or $CLMB_{T44A}$-FLAG were transfected with empty vector or pcDNA5 FRT TO encoding CNA-GFP alongside empty vector or pcDNA5 FRT TO encoding $CLMB_{WT}$-V5, $CLMB_{IxITMut}$-V5, or $CLMB_{LxVMut}$-V5. Protein expression was induced for 24 hours with 10ng/ml doxycycline, cells washed 2X in PBS and stored at -80ºC. Cells were lysed (50mM Tris pH 8, 150mM NaCl, 1% NP-40, 0.1% SDS, 0.5% sodium dodecyl sulfate, 1x Halt protease inhibitor cocktail) and resolved via SDS-PAGE and detected via immunoblotting.

In vitro CLMB phospho-peptide dephosphorylation $CLMB_{WT}$, $CLMB_{IxITMut}$, and $CLMB_{LxVMut}$ phospho-peptides were synthesized by Vivitide, resuspended in 10mM Tris pH 8.0 and dephosphorylated at 26ºC in reaction buffer (50mM Tris pH 8.0, 100mM NaCl, 6mM $MgCl_2$, 2mM $CaCl_2$, 1mM EGTA, 0.1mg/mL BSA, 1mM DTT, 0.5µM MDCC-PBP (Thermo Scientific PV4406), 1µM CaM (Millipore Sigma 208694-1MG)). Reactions were initiated by addition of CLMB peptide to a final concentration of 200nM. Reactions took place in a total of 50ml in a corning black 96 well vessel and were monitored continuously via fluorescence emitted by phosphate bound MDCC-PBP (EX:425/ EM:460). Phosphate standards were used to convert fluorescence intensity to phosphate concentration. Data were analyzed using Prism software and the rate of phosphate production was obtained by fitting data to a single exponential.

Statistical analysis
Statistical analysis was done using Graphpad Prism version 10.2.2. All data is displayed as representative images or mean values with standard deviation error bars unless otherwise noted. All data represent three independent experiments unless otherwise indicated in figure legends. Image analysis of CLMB-CN colocalization was conducted using the following number of cells: $CLMB_{WT}$ = 525, $CLMB_{IxITMut}$ = 641, $CLMB_{LxVMut}$ = 500, $CLMB_{T44A}$ = 517. Statistical significance was calculated using one-way analysis of variance (ANOVA) with corrections for multiple comparisons as indicated.

Protein expression and purification
CNAα catalytic dead mutant H151Q with an N-terminal His_6-CNA (residues 1–391) and CNB (residues 1–170) subunits were expressed using *E. coli* BL21(DE3) cells in Lysogeny Broth (LB) supplemented with 50 µg/ml ampicillin. Protein expression was induced with 1 mM isopropyl β-d-1-thiogalactopyranoside (IPTG) at 18 °C. Cells were lysed using a Fisherbrand™ Model 505 Sonic Dismembrator and lysates were centrifuged at 46,000 × *g* at 4 °C for 45 minutes. The protein was purified by incubation with nickel-nitriloacetic acid (Ni-NTA) agarose resin (Qiagen)

for 3h at 4 °C. The resin was washed with 50 mM Tris pH 8.0, 250 mM NaCl, 20 mM imidazole, and 1 mM TCEP. A buffer containing 50 mM Tris pH 8.0, 250 mM NaCl, 300 mM imidazole, and 1 mM TCEP was used for elution. CN was further purified by SEC (Superdex® 200 Increase 10/300 GL) using Phosphate-buffered saline (PBS) and $CaCl_2$ 1mM as the final buffer.

FP binding assay

All FP measurements were performed on a multifunctional microplate reader (EnVision, Perkin Elmer) in black 384-well microplates (Corning, Cat No 3575) with 30 µL of the assay solution per well. 480-nm excitation and 535-nm emission filters were used for the FP measurements. In the FP saturation binding experiments, 5nM FITC labeled peptides were mixed with increasing concentrations of calcineurin in PBS and 500 µM $CaCl_2$ buffer (from 0 to 25µM). The FP values were plotted against the log of the protein concentrations, and the dissociation constant (apparent K_D) was obtained from the resulting sigmoidal curve as analyzed in GraphPad Prism 10.

FP competition assay

For the competitive binding assay, a mixture containing 5nM FITC-labeled CLMB peptides and CN (0.08 and 2 µM for CLMB vs PVIVIT experiments) was incubated with serial dilutions of unlabeled peptides for 30 minutes at room temperature. The FP values were determined, and the IC_{50} values, i.e., the concentrations required for 50% displacement of the FITC labeled peptide, were calculated in GraphPad Prism 10. The K_i values of competitive inhibitors were calculated based on a previously reported method[30], further adapted by[31]. Briefly, the relation of K_i and IC_{50} in competitive inhibition as applied to protein-ligand–inhibitor (P–L–I) interactions, can be summarized by the following equation:

$$K_i = \frac{IC_{50}}{(\frac{\mathrm{L}}{K_d} + 1)}$$

Where L stands for the concentration of ligand, i.e., the FITC-labeled peptide used in the FP binding assay; and K_D corresponds to the dissociation constant of the same FITC-labeled peptide resulting from the performed FP binding assay.

ITC measurements

Isothermal titration calorimetry (ITC) experiments were performed using an Affinity ITC from TA Instruments (New Castle, DE) equipped with an autosampler in a buffer containing 50 mM HEPES, pH 8.0, 150 mM NaCl, 1 mM TCEP, 500µM $CaCl_2$ at 25 °C. 40 µM protein solution in the calorimetric cell was titrated with 100 µM peptide solution using 0.5 µL injection in 200-sec intervals using stirring speed at 125rpm. The resulting isotherm was fitted with a single site model to yield thermodynamic parameters of ΔH, ΔS, stoichiometry, and K_D using NanoAnalyze software (TA instruments).

Antibodies:

Mouse anti-FLAG 1:2500
https://www.sigmaaldrich.com/US/en/product/sigma/F3165
Rabbit anti-GFP 1:1000
https://www.thermofisher.com/antibody/product/GFP-Antibody-Polyclonal/A-11122
Mouse anti-GAPDH 1:2000
https://www.scbt.com/p/gapdh-antibody-g-9
Mouse anti-V5 1:5000
https://www.thermofisher.com/antibody/product/V5-Tag-Antibody-clone-SV5-Pk1-Monoclonal/R960-25
Rabbit anti-calnexin 1:2500

(https://www.enzolifesciences.com/ADI-SPA-865/calnexin-polyclonal-antibody/)
Mouse anti-GM130 1:3000
https://www.cellsignal.com/products/primary-antibodies/gm130-d6b1-xp-rabbit-mab/12480
Rabbit anti-αTubulin 1:2000
https://www.sigmaaldrich.com/US/en/product/sigma/t9026
Chicken anti-GFP 1:100
https://www.novusbio.com/products/gfp-antibody_nb100-1614
Rabbit anti-FLAG: 1:100 IF 1:1000 WB
https://www.sigmaaldrich.com/US/en/product/sigma/F7425
TRITC tagged Goat anti-rabbit 1:100
https://biotium.com/product/goat-anti-rabbit-igg-hl-highly-cross-absorbed/?attribute_pa_conjugation=cf555
A488 tagged goat anti-chicken 1:100
https://biotium.com/product/goat-anti-chicken-igy-igg-hl-highly-cross-adsorbed/?attribute_pa_conjugation=cf488a
Licor Rabbit 800
https://www.licor.com/bio/reagents/irdye-800cw-goat-anti-rabbit-igg-secondary-antibody
Licor Mouse 680
https://www.licor.com/bio/reagents/irdye-680rd-goat-anti-mouse-igg-secondary-antibody
Licor Strep 800
https://www.licor.com/bio/reagents/irdye-800cw-streptavidin

Plasmids:

Construct	Backbone	Plasmid Number	Primer 1	Primer 2	Note
$CLMB_{WT}$-FLAG	pcDNA5/FRT/TO	2801	DB29	DB30	C16-BamHI-GFP-Xho starting point. GFP cut out and replaced with pre-annealed BamH1-FLAG-XhoI to FLAG tag C16
$CLMB_{IxITMut}$-FLAG	pcDNA5/FRT/TO	2862	CPW239	CPW240	QC
$CLMB_{LxVMut}$-FLAG	pcDNA5/FRT/TO	2861	DB10	DB11	QC
$CLMB_{T44A}$-FLAG	pcDNA5/FRT/TO	2860	DBT44A-F	DBT44A-R	QC
$CLMB_{LxVMut+T44A}$-FLAG	pcDNA3	2852	DBT44A-F	DBT44A-R	QC
$CLMB_{C7S}$-FLAG	pcDNA5/FRT/TO	2863	DB14	DB15	QC
$CLMB_{C7,14S}$-FLAG	pcDNA5/FRT/TO	2880	DB23	DB24	QC
$CLMB_{G2A}$-FLAG	pcDNA5/FRT/TO	2864	DB31	DB32	QC
CLMBWT-V5	pcDNA5/FRT/TO	2918	DB53	DB54	Cloned HindIII-C16-V5-XhoI out of the split turbo construct and inserted it into DB35 after cutting C16-FLAG out

CLMBIxIT Mut-V5	pcDNA5/FRT/TO	3125	CPW239CPW240		QC
CNA-GFP	pcDNA5/FRT/TO	2683			I didn't make
6xHis-CNA_{FL}/CNB	p11	1447			I didn't make
6xHis-CNA_{FL+NIR}/CNB	p11	3189	DB169	DB170	QC

Acknowledgements

We thank Norman Davey and members of the Cyert and Arthanari labs, in particular Angela Barth, for helpful discussion. We are grateful to Callie Wigington, Makena Pule, Thibault Viennet and Shariq Qayyum for their early contributions to the project. We thank Ilya Bezprozvanny for suggesting the name, calcimembrin.

Funding

MSC and DAB are supported by NIH grant R35 GM136243. DAB also acknowledges support from NIH grant T32 GM007276. HA and JCR received funding from NIH grant R01 GM136859.

Author Contributions

All authors conceived the studies. DAB, supervised by MSC, carried out experiments and analyzed data except for Figure 3, and prepared figures. JCR, supervised by HA, carried out experiments and analyzed data for Figure 3. DAB and MSC wrote the manuscript in consultation with HA and JCR.

References

1. Ulengin-Talkish I, Cyert MS. A cellular atlas of calcineurin signaling. Biochim Biophys Acta Mol Cell Res. 2023;1870(1):119366. Epub 2022/10/04. doi: 10.1016/j.bbamcr.2022.119366. PubMed PMID: 36191737; PMCID: PMC9948804.
2. Li H, Pink MD, Murphy JG, Stein A, Dell'Acqua ML, Hogan PG. Balanced interactions of calcineurin with AKAP79 regulate Ca2+-calcineurin-NFAT signaling. Nature structural & molecular biology. 2012;19(3):337-45. doi: 10.1038/nsmb.2238. PubMed PMID: 22343722; PMCID: 3294036.
3. Aramburu J, Rao A, Klee CB. Calcineurin: from structure to function. Curr Top Cell Regul. 2000;36:237-95. PubMed PMID: 10842755.
4. Grigoriu S, Bond R, Cossio P, Chen JA, Ly N, Hummer G, Page R, Cyert MS, Peti W. The molecular mechanism of substrate engagement and immunosuppressant inhibition of calcineurin. PLoS Biol. 2013;11(2):e1001492. doi: 10.1371/journal.pbio.1001492. PubMed PMID: 23468591; PMCID: 3582496.

5. Roy J, Cyert MS. Identifying New Substrates and Functions for an Old Enzyme: Calcineurin. Cold Spring Harb Perspect Biol. 2020;12(3). Epub 2019/07/17. doi: 10.1101/cshperspect.a035436. PubMed PMID: 31308145; PMCID: PMC7050593.
6. Brauer BL, Moon TM, Sheftic SR, Nasa I, Page R, Peti W, Kettenbach AN. Leveraging New Definitions of the LxVP SLiM To Discover Novel Calcineurin Regulators and Substrates. ACS Chem Biol. 2019;14(12):2672-82. Epub 2019/10/22. doi: 10.1021/acschembio.9b00606. PubMed PMID: 31633908; PMCID: PMC6925343.
7. Sheftic SR, Page R, Peti W. Investigating the human Calcineurin Interaction Network using the piLxVP SLiM. Scientific reports. 2016;6:38920. doi: 10.1038/srep38920. PubMed PMID: 27974827; PMCID: 5156906.
8. Tsekitsidou E, Wong CJ, Ulengin-Talkish I, Barth AIM, Stearns T, Gingras AC, Wang JT, Cyert MS. Calcineurin associates with centrosomes and regulates cilia length maintenance. Journal of cell science. 2023;136(8). Epub 2023/04/05. doi: 10.1242/jcs.260353. PubMed PMID: 37013443; PMCID: PMC10163345.
9. Wigington CP, Roy J, Damle NP, Yadav VK, Blikstad C, Resch E, Wong CJ, Mackay DR, Wang JT, Krystkowiak I, Bradburn DA, Tsekitsidou E, Hong SH, Kaderali MA, Xu SL, Stearns T, Gingras AC, Ullman KS, Ivarsson Y, Davey NE, Cyert MS. Systematic Discovery of Short Linear Motifs Decodes Calcineurin Phosphatase Signaling. Molecular cell. 2020;79(2):342-58 e12. Epub 2020/07/10. doi: 10.1016/j.molcel.2020.06.029. PubMed PMID: 32645368; PMCID: PMC7416808.
10. Nakamura T, Katagiri T, Sato S, Kushibiki T, Hontani K, Tsuchikawa T, Hirano S, Nakamura Y. Overexpression of C16orf74 is involved in aggressive pancreatic cancers. Oncotarget. 2017;8(31):50460-75. Epub 2016/07/28. doi: 10.18632/oncotarget.10912. PubMed PMID: 28881575; PMCID: PMC5584151.
11. Uhlen M, Oksvold P, Fagerberg L, Lundberg E, Jonasson K, Forsberg M, Zwahlen M, Kampf C, Wester K, Hober S, Wernerus H, Bjorling L, Ponten F. Towards a knowledge-based Human Protein Atlas. Nat Biotechnol. 2010;28(12):1248-50. Epub 2010/12/09. doi: 10.1038/nbt1210-1248. PubMed PMID: 21139605.
12. Mesquita, FS, Abrami L, Linder ME, Bamji SX, Dickinson BC, van der Goot FG. Mechanisms and functions of protein S-acylation. Nat Rev Mol Cell Biol. 2024. Epub 2024/02/15. doi: 10.1038/s41580-024-00700-8. PubMed PMID: 38355760.
13. Chen X, Crosby KC, Feng A, Purkey AM, Aronova MA, Winters CA, Crocker VT, Leapman RD, Reese TS, Dell'Acqua ML. Palmitoylation of A-kinase anchoring protein 79/150 modulates its nanoscale organization, trafficking, and mobility in postsynaptic spines. Front Synaptic Neurosci. 2022;14:1004154. Epub 2022/10/04. doi: 10.3389/fnsyn.2022.1004154. PubMed PMID: 36186623; PMCID: PMC9521714.
14. Ulengin-Talkish I, Parson MAH, Jenkins ML, Roy J, Shih AZL, St-Denis N, Gulyas G, Balla T, Gingras AC, Varnai P, Conibear E, Burke JE, Cyert MS. Palmitoylation targets the calcineurin phosphatase to the phosphatidylinositol 4-kinase complex at the plasma membrane. Nat Commun. 2021;12(1):6064. Epub 2021/10/20. doi: 10.1038/s41467-021-26326-4. PubMed PMID: 34663815; PMCID: PMC8523714.
15. Rual JF, Venkatesan K, Hao T, Hirozane-Kishikawa T, Dricot A, Li N, Berriz GF, Gibbons FD, Dreze M, Ayivi-Guedehoussou N, Klitgord N, Simon C, Boxem M, Milstein S, Rosenberg J, Goldberg DS, Zhang LV, Wong SL, Franklin G, Li S, Albala JS, Lim J, Fraughton C, Llamosas E, Cevik S, Bex C, Lamesch P, Sikorski RS, Vandenhaute J, Zoghbi HY, Smolyar A, Bosak S, Sequerra R, Doucette-Stamm L, Cusick ME, Hill DE, Roth FP, Vidal M. Towards a proteome-scale map of the human protein-protein interaction network. Nature. 2005;437(7062):1173-8. doi: 10.1038/nature04209. PubMed PMID: 16189514.
16. Meinnel T, Dian C, Giglione C. Myristoylation, an Ancient Protein Modification Mirroring Eukaryogenesis and Evolution. Trends Biochem Sci. 2020;45(7):619-32. Epub 2020/04/20. doi: 10.1016/j.tibs.2020.03.007. PubMed PMID: 32305250.

17. Blanc M, David FPA, van der Goot FG. SwissPalm 2: Protein S-Palmitoylation Database. Methods Mol Biol. 2019;2009:203-14. Epub 2019/06/04. doi: 10.1007/978-1-4939-9532-5_16. PubMed PMID: 31152406.
18. Kushibiki T, Nakamura T, Tsuda M, Tsuchikawa T, Hontani K, Inoko K, Takahashi M, Asano T, Okamura K, Murakami S, Kurashima Y, Ebihara Y, Noji T, Nakanishi Y, Tanaka K, Maishi N, Sasaki K, Park WR, Shichinohe T, Hida K, Tanaka S, Hirano S. Role of Dimerized C16orf74 in Aggressive Pancreatic Cancer: A Novel Therapeutic Target. Mol Cancer Ther. 2020;19(1):187-98. Epub 2019/10/11. doi: 10.1158/1535-7163.MCT-19-0491. PubMed PMID: 31597713.
19. Yap MC, Kostiuk MA, Martin DD, Perinpanayagam MA, Hak PG, Siddam A, Majjigapu JR, Rajaiah G, Keller BO, Prescher JA, Wu P, Bertozzi CR, Falck JR, Berthiaume LG. Rapid and selective detection of fatty acylated proteins using omega-alkynyl-fatty acids and click chemistry. Journal of lipid research. 2010;51(6):1566-80. Epub 2009/12/24. doi: 10.1194/jlr.D002790. PubMed PMID: 20028662; PMCID: PMC3035521.
20. Percher A, Ramakrishnan S, Thinon E, Yuan X, Yount JS, Hang HC. Mass-tag labeling reveals site-specific and endogenous levels of protein S-fatty acylation. Proceedings of the National Academy of Sciences of the United States of America. 2016;113(16):4302-7. doi: 10.1073/pnas.1602244113. PubMed PMID: 27044110; PMCID: 4843475.
21. Dekker FJ, Rocks O, Vartak N, Menninger S, Hedberg C, Balamurugan R, Wetzel S, Renner S, Gerauer M, Scholermann B, Rusch M, Kramer JW, Rauh D, Coates GW, Brunsveld L, Bastiaens PI, Waldmann H. Small-molecule inhibition of APT1 affects Ras localization and signaling. Nat Chem Biol. 2010;6(6):449-56. Epub 2010/04/27. doi: 10.1038/nchembio.362. PubMed PMID: 20418879.
22. Perrino BA, Ng LY, Soderling TR. Calcium regulation of calcineurin phosphatase activity by its B subunit and calmodulin. Role of the autoinhibitory domain. The Journal of biological chemistry. 1995;270(1):340-6. Epub 1995/01/06. doi: 10.1074/jbc.270.1.340. PubMed PMID: 7814394.
23. Aramburu J, Yaffe MB, Lopez-Rodriguez C, Cantley LC, Hogan PG, Rao A. Affinity-driven peptide selection of an NFAT inhibitor more selective than cyclosporin A. Science. 1999;285:2129-33.
24. Li H, Zhang L, Rao A, Harrison SC, Hogan PG. Structure of calcineurin in complex with PVIVIT peptide: portrait of a low-affinity signalling interaction. Journal of molecular biology. 2007;369(5):1296-306. PubMed PMID: 17498738.
25. Nguyen HQ, Roy J, Harink B, Damle NP, Latorraca NR, Baxter BC, Brower K, Longwell SA, Kortemme T, Thorn KS, Cyert MS, Fordyce PM. Quantitative mapping of protein-peptide affinity landscapes using spectrally encoded beads. eLife. 2019;8. Epub 2019/07/10. doi: 10.7554/eLife.40499. PubMed PMID: 31282865; PMCID: PMC6728138.
26. Huang CH, Chen YC, Chen CC. Physical interaction between calcineurin and Cav3.2 T-type Ca2+ channel modulates their functions. FEBS Lett. 2013;587(12):1723-30. Epub 2013/05/15. doi: 10.1016/j.febslet.2013.04.040. PubMed PMID: 23669360.
27. Lee S, Lee HT, Kim YA, Lee IH, Kang SJ, Sim K, Park CG, Choi K, Youn HD. The optimized core peptide derived from CABIN1 efficiently inhibits calcineurin-mediated T-cell activation. Exp Mol Med. 2022;54(5):613-25. Epub 2022/05/14. doi: 10.1038/s12276-022-00772-6. PubMed PMID: 35550603; PMCID: PMC9166766.
28. Johnson JL, Yaron TM, Huntsman EM, Kerelsky A, Song J, Regev A, Lin TY, Liberatore K, Cizin DM, Cohen BM, Vasan N, Ma Y, Krismer K, Robles JT, van de Kooij B, van Vlimmeren AE, Andree-Busch N, Kaufer NF, Dorovkov MV, Ryazanov AG, Takagi Y, Kastenhuber ER, Goncalves MD, Hopkins BD, Elemento O, Taatjes DJ, Maucuer A, Yamashita A, Degterev A, Uduman M, Lu J, Landry SD, Zhang B, Cossentino I, Linding R, Blenis J, Hornbeck PV, Turk BE, Yaffe MB, Cantley LC. An atlas of substrate specificities for the human serine/threonine

kinome. Nature. 2023;613(7945):759-66. Epub 2023/01/12. doi: 10.1038/s41586-022-05575-3. PubMed PMID: 36631611; PMCID: PMC9876800
29. Stirling DR, Swain-Bowden MJ, Lucas AM, Carpenter AE, Cimini BA, Goodman A. CellProfiler 4: improvements in speed, utility and usability. BMC Bioinformatics. 2021;22(1):433. Epub 2021/09/12. doi: 10.1186/s12859-021-04344-9. PubMed PMID: 34507520; PMCID: PMC8431850.
30. Cheng Y, Prusoff WH. Relationship between the inhibition constant (K1) and the concentration of inhibitor which causes 50 per cent inhibition (I50) of an enzymatic reaction. Biochem Pharmacol. 1973;22(23):3099-108. Epub 1973/12/01. doi: 10.1016/0006-2952(73)90196-2. PubMed PMID: 4202581.
31. Cer RZ, Mudunuri U, Stephens R, Lebeda FJ. IC50-to-Ki: a web-based tool for converting IC50 to Ki values for inhibitors of enzyme activity and ligand binding. Nucleic acids research. 2009;37(Web Server issue):W441-5. Epub 2009/04/28. doi: 10.1093/nar/gkp253. PubMed PMID: 19395593; PMCID: PMC2703898.

Figure legends

Figure 1: Calcimembrin localizes to membranes via protein lipidation.
a Schematic of Clmb. N-myristoylation (red); S-acylated cysteines (yellow); T44 phospho-threonine (green); Cn binding motifs LxVP (pink) and PxIxIT (purple). Mutant sequences shown for $CLMB_{LxVMut}$ and $CLMB_{IXITMut.}$

b Clmb incorporates analogs of palmitate (17-ODYA) or myristate (YnMyr) as indicated. Cells were treated with 20μM MG132 prior to harvesting. Representative immunoblot shown of FLAG tagged Clmb wild type ($CLMB_{WT}$), palmitoylation defective ($CLMB_{C7,14S}$) or myristoylation defective ($CLMB_{G2A}$), immunoprecipitated and detected using CLICK chemistry with Biotin-Azide followed by detection with IRdye 800CW streptavidin (n = 3 independent experiments). Asterisks indicate Clmb dimers formed due to absence of reducing agents (see methods).

c Representative immunoblot of acyl-PEG exchange performed on lysates expressing $CLMB_{WT}$-FLAG or lipidation mutants ($CLMB_{C7S}$, $CLMB_{C7,14S}$, $CLMB_{G2A}$). PEGylation events, a proxy for S-acylation are indicated by asterisks. For each sample, input, cleaved (NH_2OH) and PEGylated (mPEG), and non-cleaved PEGylated conditions are shown. Cells were treated with 20μM MG132 for 4 hours prior to harvesting. Endogenous, dually palmitoylated calnexin is a positive control (n = 3 independent experiments).

d Pulse chase analysis of CLMB-FLAG S-acylation turnover using analogs of palmitate (17-ODYA) or methionine (L-AHA). Incorporation into immunoprecipitated CLMB-FLAG in the absence of analog (Neg Ctrl), or after 2 hours of analog treatment followed by 0 or 30 minute without analog including DMSO (control) or palmostatin B. 17-ODYA or L-AHA were detected using CLICK with Cy5 and AZDye 488, respectively. A representative in-gel fluorescence scan is shown (n = 3 independent experiments).

e Data from (**d**) showing mean ± SEM of 17-ODYA signal normalized to L-AHA. Indicated p-values calculated by two-way ANOVA corrected by Tukey's multiple comparison test. N=3 independent experiments.

f Sub-cellular fractionation of lysates containing $CLMB_{WT}$-FLAG or lipidation mutants ($CLMB_{C7,14S}$, $CLMB_{G2A}$). Cells were treated with 20μM MG132 for 4 hours prior to harvesting.

Representative immunoblot showing input, cytoplasmic (cyto), and membrane (mem) fractions. GM130 and α-tubulin mark membrane and cytosolic fractions respectively.

g Data from (**f)** showing mean ± SEM cytoplasmic or membrane signals normalized to total (cytoplasmic + membrane signals). Indicated p-values calculated by two-way ANOVA corrected by Tukey's multiple comparison test. N= 3 independent experiments.

Figure 2: Composite SLiM in calcimembrin mediates binding to and dephosphorylation by calcineurin

a Representative immunoblot of anti-GFP purification from lysates of HEK293 cells co-transfected with CNA-GFP and CLMB-FLAG ($CLMB_{WT}$, $CLMB_{IxITMut}$, $CLMB_{LxVMut}$, $CLMB_{T44A}$, or $CLMB_{LxVMut+T44A}$).

b Data from (**a**) showing mean ± SEM CLMB-FLAG pulled down normalized to CLMB-FLAG input levels and CNA-GFP pulled down. Indicated p-values calculated by two-way ANOVA corrected by Dunnett's multiple comparison test (n = 3 independent experiments).

c Representative immunofluorescence images of fixed MCF7 cells co-transfected with CLMB-FLAG ($CLMB_{WT}$, $CLMB_{IxITMut}$, $CLMB_{LxVMut}$, or $CLMBn_{T44A}$) and CNA-GFP. CLMB was visualized using anti-FLAG, CN with anti-GFP, and nuclei with Hoechst 33342. Scale bar = 50 µm.

d Data from (**c**) showing median with 95% CI Pearson's correlation coefficient of CLMB-CN colocalization. Each point represents a single cell (n ≥ 500 for each condition). Indicated p-values calculated by Kruskal-Wallis with Dunn's multiple comparisons correction.

e Plot of phosphate released from 200 nM $pCLMB_{WT}$ (blue circles) or $pCLMB_{LxVMut}$ (pink squares) phospho-peptides dephosphorylated by 20 nM CN and 1 µM CaM. Displayed is the mean ± SEM of phosphate released for ≥ 4 replicates at each timepoint.

Figure 3: Phosphorylation and the LxVP motif contribute to PxIxIT binding.

a Isothermal calorimetric enthalpy change displaying the thermometric evaluation of the affinity between CN A/B complex and unlabeled pWT peptide (top), and binding isotherm obtained by titration of unlabeled pWT into calcineurin A/B complex (40 µM) (bottom). A dissociation constant (K_D) = 8.3 ± 5.7 nM was obtained.

b Fluorescence polarization (FP) saturation binding curves of two different FITC-labeled peptide tracers (5nM), FITC-$pCLMB_{WT}$ and FITC-$CLMB_{WT}$ were incubated with serial dilutions of CN A/B complex (0 to 12.5µM). The FP values were recorded at room temperature after a 30-minute incubation time. FP data were fitted to a one-site binding model (mean ± s.d., n = 2 independent experiments) using GraphPad Prism 10.0.

c Competitive binding assay of unlabeled $pCLMB_{WT}$, $CLMB_{WT}$, $pCLMB_{IxITMut}$, and $pCLMB_{LxVMut}$ peptides. The unlabeled peptides were titrated against a constant concentration of FP probe (FITC-PVIVIT peptide, 5 nM) in the presence of 2 µM CN A/B complex. Data (mean ± s.d., n = 2 independent experiments) were analyzed in GraphPad Prism 10.0.

d Competitive binding assay of unlabeled $pCLMB_{WT}$, $CLMB_{WT}$, $pCLMB_{IxITMut}$, and $pCLMB_{LxVMut}$ peptides. The unlabeled peptides were titrated against a constant concentration of FP probe (FITC-$pCLMB_{WT}$ peptide, 5 nM) in the presence of 0.08 µM CN A/B complex. Data (mean ± s.d., n = 2 independent experiments) were analyzed in GraphPad Prism 10.0.

e Table displaying the experimentally obtained IC_{50} values and converted K_i values resulting from the competitive binding assay of unlabeled $pCLMB_{WT}$, $CLMB_{WT}$, $pCLMB_{IxITMut}$, and $pCLMB_{LxVMut}$ peptides. The unlabeled peptides were titrated against a constant concentration of FP probe (FITC-$pCLMB_{WT}$ or FITC-PVIVIT, 5 nM) in the presence of 0.08μM and 2μM CN A/B complex, respectively. Data (mean ± s.d., n = 2 independent experiments) were analyzed in GraphPad Prism 10.0.

Figure 4: Calcineurin dephosphorylates calcimembrin by forming multimers.
a Representative immunoblot of CLMB-FLAG phosphorylation-induced mobility shifts induced by CN overexpression. Performed using lysates from Flp-In-T-REx HEK cells inducibly expressing $CLMB_{WT}$-FLAG or $CLMB_{IxITMut}$-FLAG and transfected with empty vector, CNA-GFP, or CNA-GFP with CLMB-V5 ($CLMB_{WT}$, $CLMB_{IxITMut}$, $CLMB_{LxVMut}$). Asterisks indicate phosphorylated CLMB.

b Data from (**a**) showing mean ± SEM phospho-CLMB-FLAG normalized to total CLMB-FLAG. Displayed p-values calculated by two-way ANOVA corrected by Dunnett's multiple comparison test (n = 3 independent experiments).

c Plots of phosphate released from 200 nM $pCLMB_{WT}$ phosphopeptide dephosphorylated by 20nm (green triangle), 100nM (blue square) or 200nM (purple circle) CN and 1μM calmodulin. Displayed is the mean ± SEM of phosphate released for ≥ 4 replicates at each timepoint.

d Plots of phosphate released from 200 nM $pCLMB_{IxITMut}$ phosphopeptide dephosphorylated by 20nm (green triangle), 100nM (blue square) or 200nM (purple circle) CN and 1μM calmodulin. Displayed is the mean ± SEM of phosphate released for ≥ 3 replicates at each timepoint.

e. Dephosphorylation rates determined for experiments in (**c**) and (**d**) using one phase association analysis in GraphPad Prism version 10.2.2.

Figure 5: A model for how calcimembrin modulates calcineurin signaling.
a (1) CLMB is dynamically acylated and localizes to membranes where it (2) recruits CN. When CLMB levels are low, CN remains tightly bound to phosphorylated CLMB regardless of Ca^{2+} signals. (3) As CLMB levels rise, Ca^{2+} and CaM binding allow CN-CLMB multimers to form and CLMB to be dephosphorylated. (4) CN is then freed to engage and dephosphorylate nearby substrates, activating CN signaling.

b (1) CLMB is dynamically acylated and localizes to membranes where it (2) recruits CN. When CLMB levels are low, CN remains tightly bound to phosphorylated CLMB. (3) Ca^{2+} and CaM activate CN, allowing CLMB to present it to nearby substrates for LxVP-mediated binding and dephosphorylation. (4) When CLMB accumulates at membranes, CN-CLMB multimers form, and (5) dephosphorylation triggers CN release, terminating CN signaling.

A

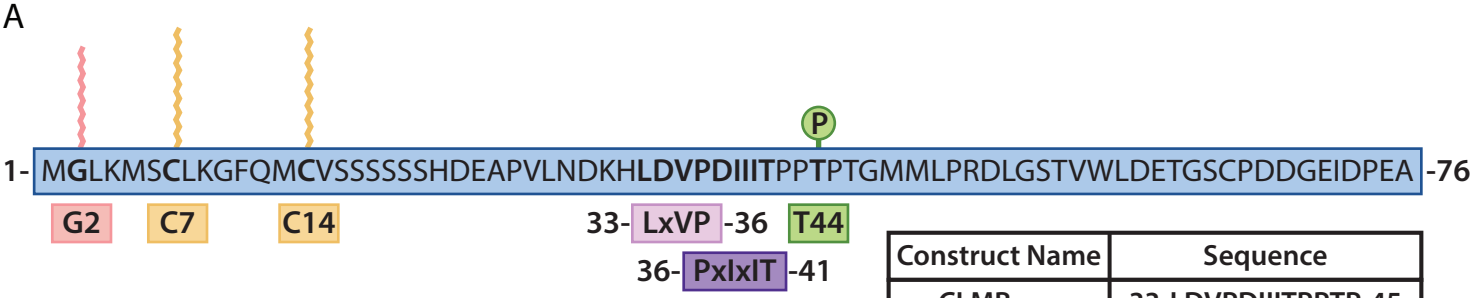

Construct Name	Sequence
$CLMB_{WT}$	33-LDVPDIIITPPTP-45
$CLMB_{LxVMut}$	33-ADAPDIIITPPTP-45
$CLMB_{IxITMut}$	33-LDVPDAIAAPPTP-45

B

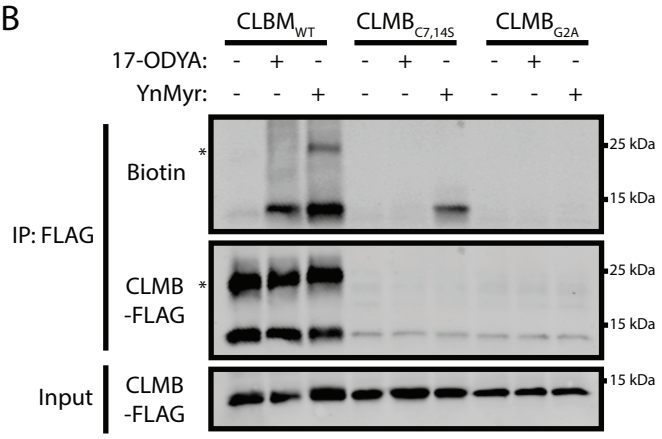

C

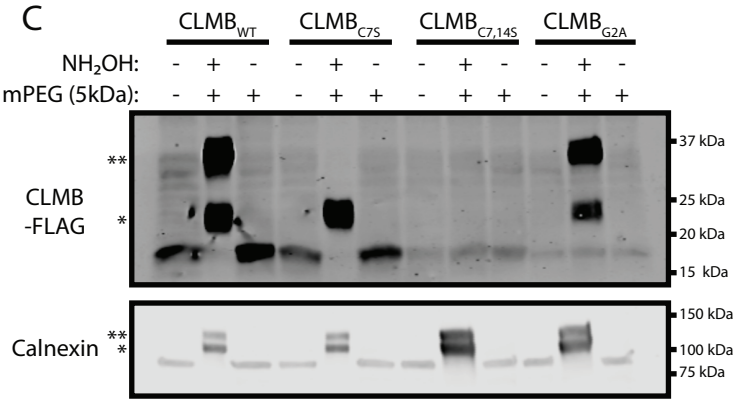

D

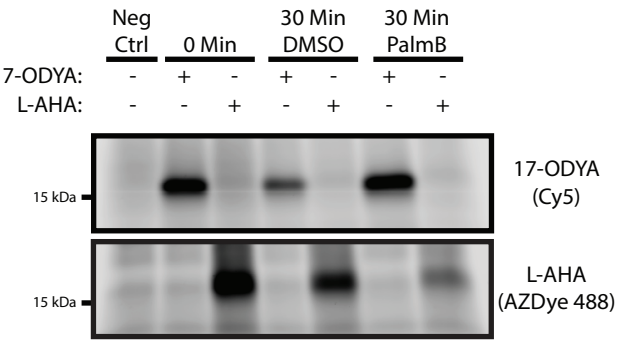

E

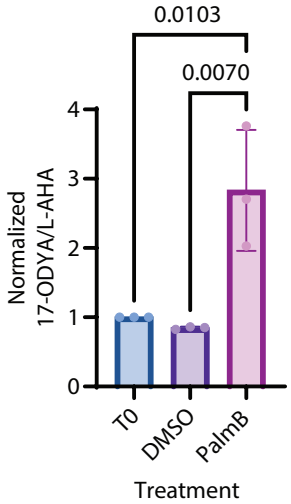

F

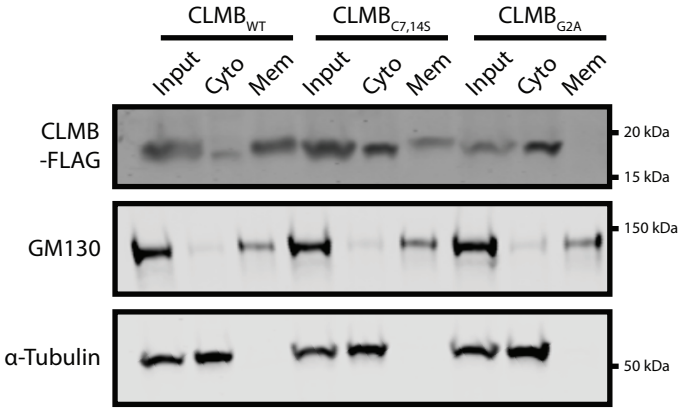

G

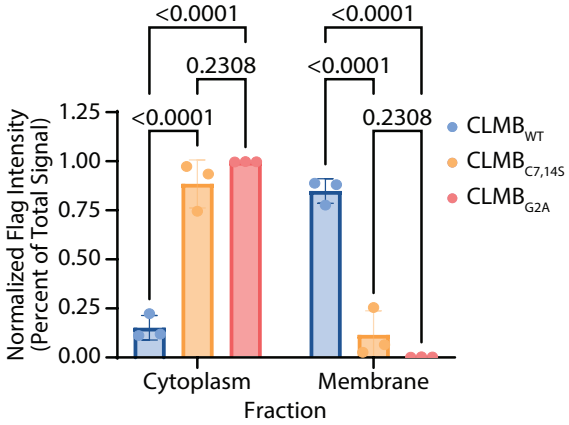

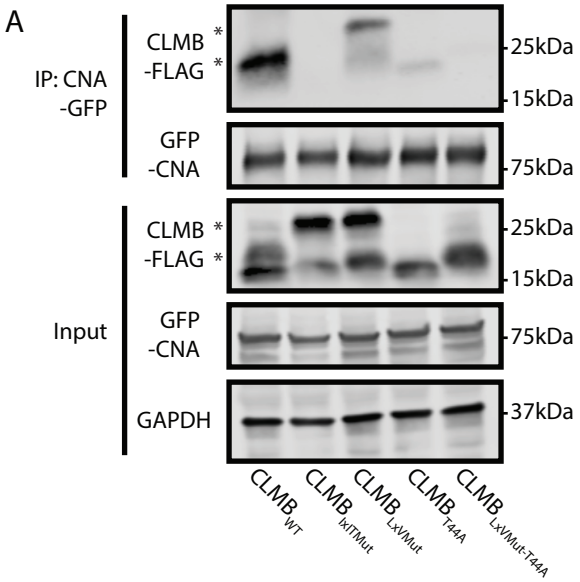
A
IP: CNA
-GFP
CLMB
-FLAG
GFP
-CNA
Input
CLMB
-FLAG
GFP
-CNA
GAPDH
25kDa
15kDa
75kDa
25kDa
15kDa
75kDa
37kDa
CLMB WT
CLMB IxITMut
CLMB LxVMut
CLMB T44A
CLMB LxVMut-T44A

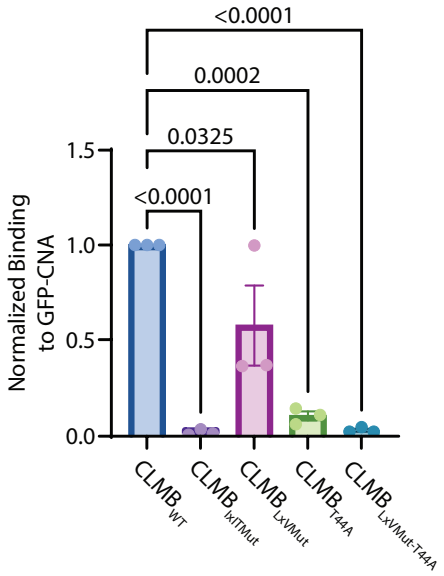
B
<0.0001
0.0002
0.0325
<0.0001
Normalized Binding
to GFP-CNA
1.5
1.0
0.5
0.0
CLMB WT
CLMB IxITMut
CLMB LxVMut
CLMB T44A
CLMB LxVMut-T44A

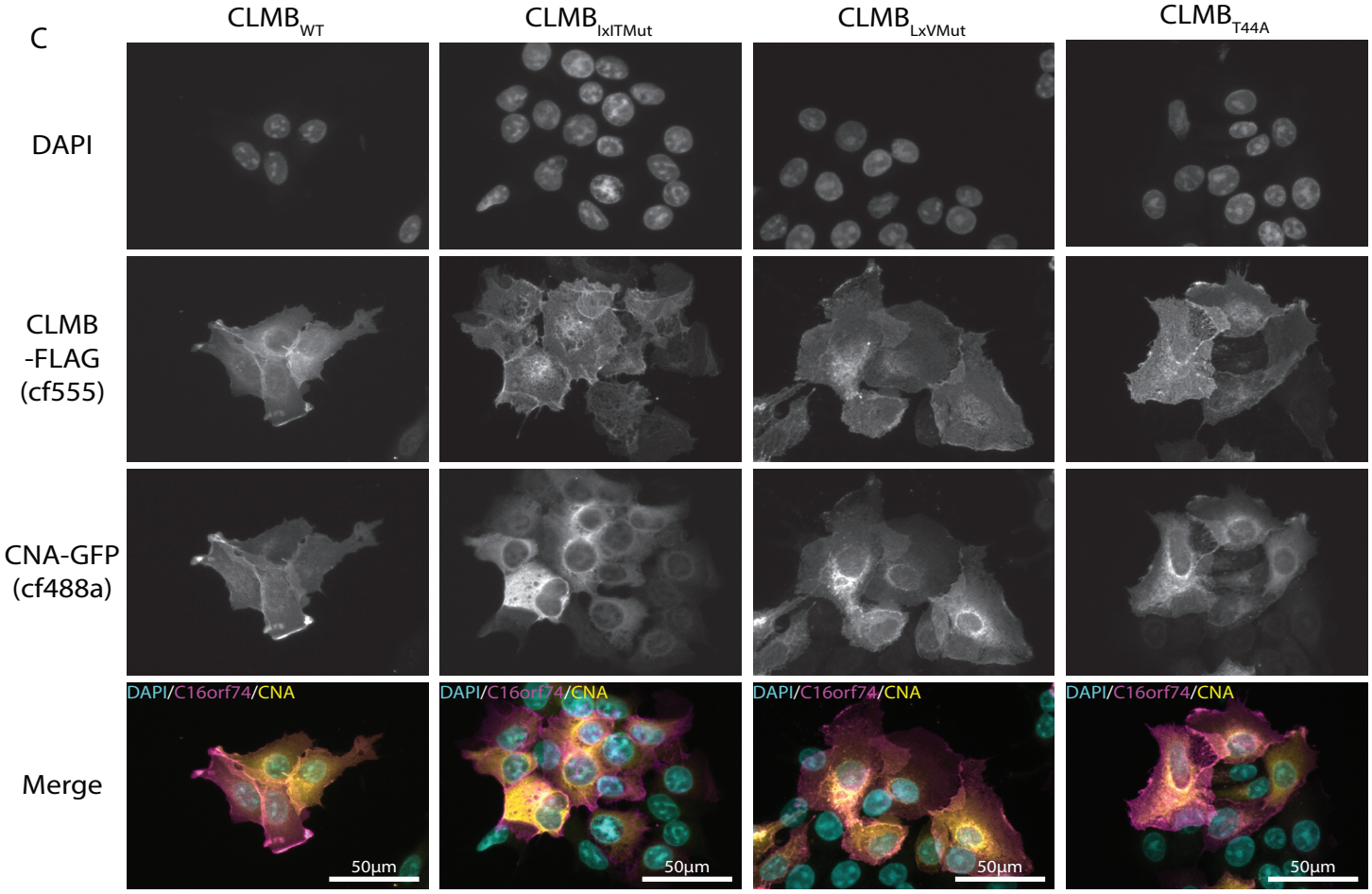
C
CLMB WT
CLMB IxITMut
CLMB LxVMut
CLMB T44A
DAPI
CLMB
-FLAG
(cf555)
CNA-GFP
(cf488a)
Merge
DAPI/C16orf74/CNA
50µm

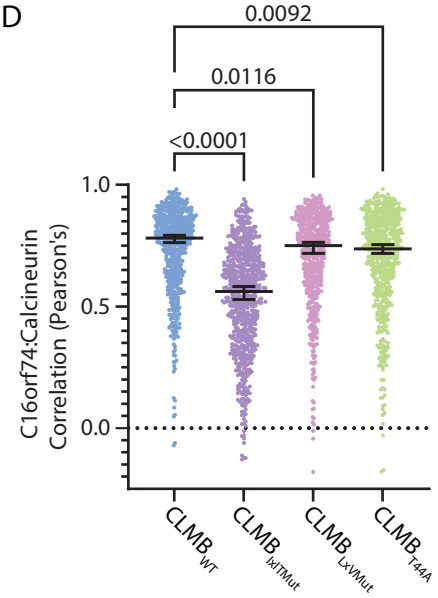
D
0.0092
0.0116
<0.0001
C16orf74:Calcineurin
Correlation (Pearson's)
1.0
0.5
0.0
CLMB WT
CLMB IxITMut
CLMB LxVMut
CLMB T44A

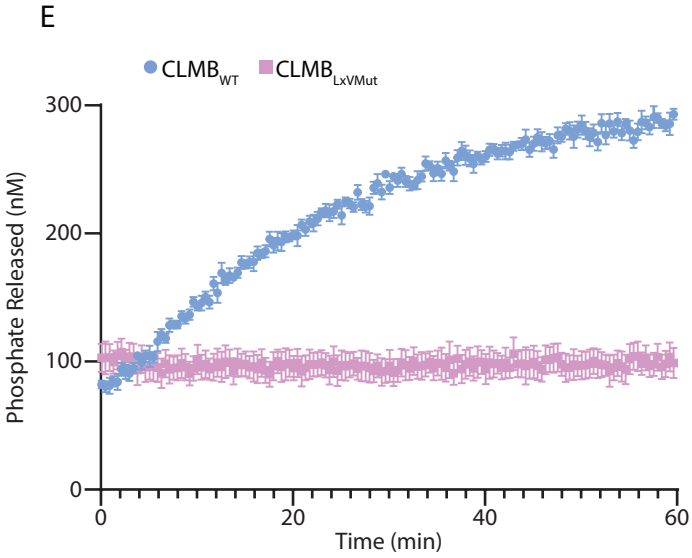
E
CLMB WT
CLMB LxVMut
Phosphate Released (nM)
300
200
100
0
0
20
40
60
Time (min)

A

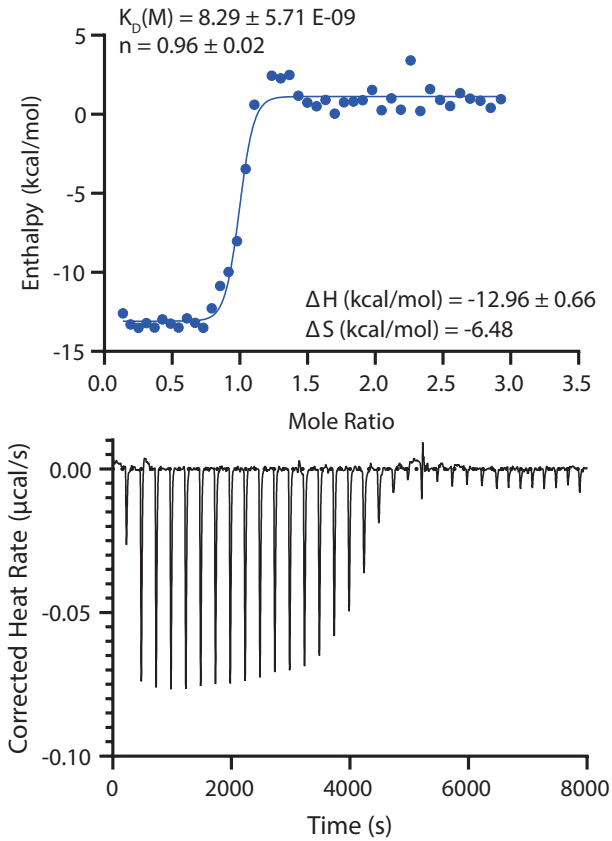

B

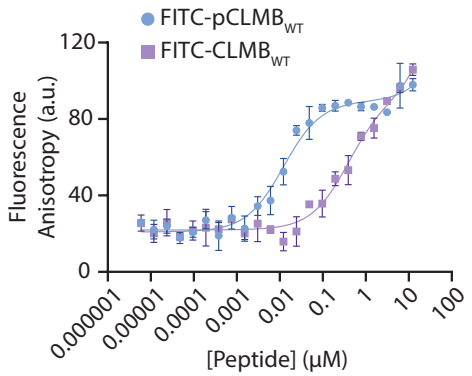

C

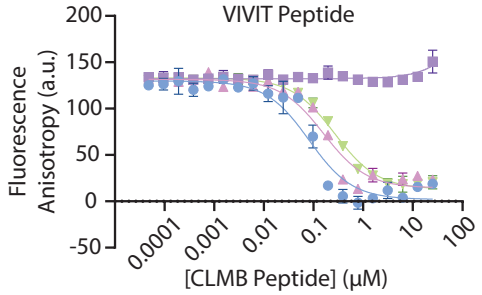

D

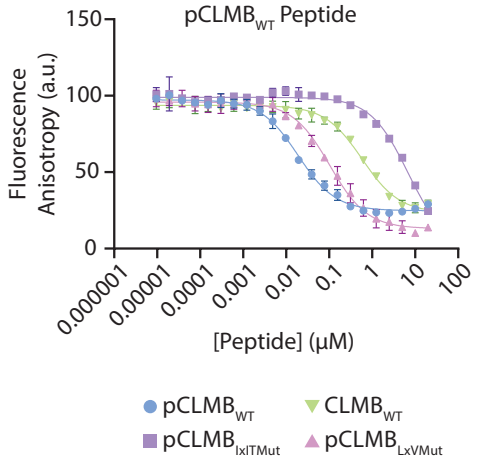

E

Peptide Competitor	FITC-VIVIT		FITC-pCLMB$_{WT}$	
	IC_{50}(µM)	K_i (µM)	IC_{50}(µM)	K_i (µM)
pCLMB$_{WT}$	81.4 ± 16.2	80.9 ± 16.1	18.9 ± 1.2	13.4 ± 0.8
pCLMB$_{IxITMut}$	NA	NA	6687 ± 878	4754 ± 624
pCLMB$_{LxVMut}$	159 ± 30	158± 30	103 ± 9	73.2 ± 6.4
CLMB$_{WT}$	267 ± 21	265 ± 21	585 ± 57	426 ± 40

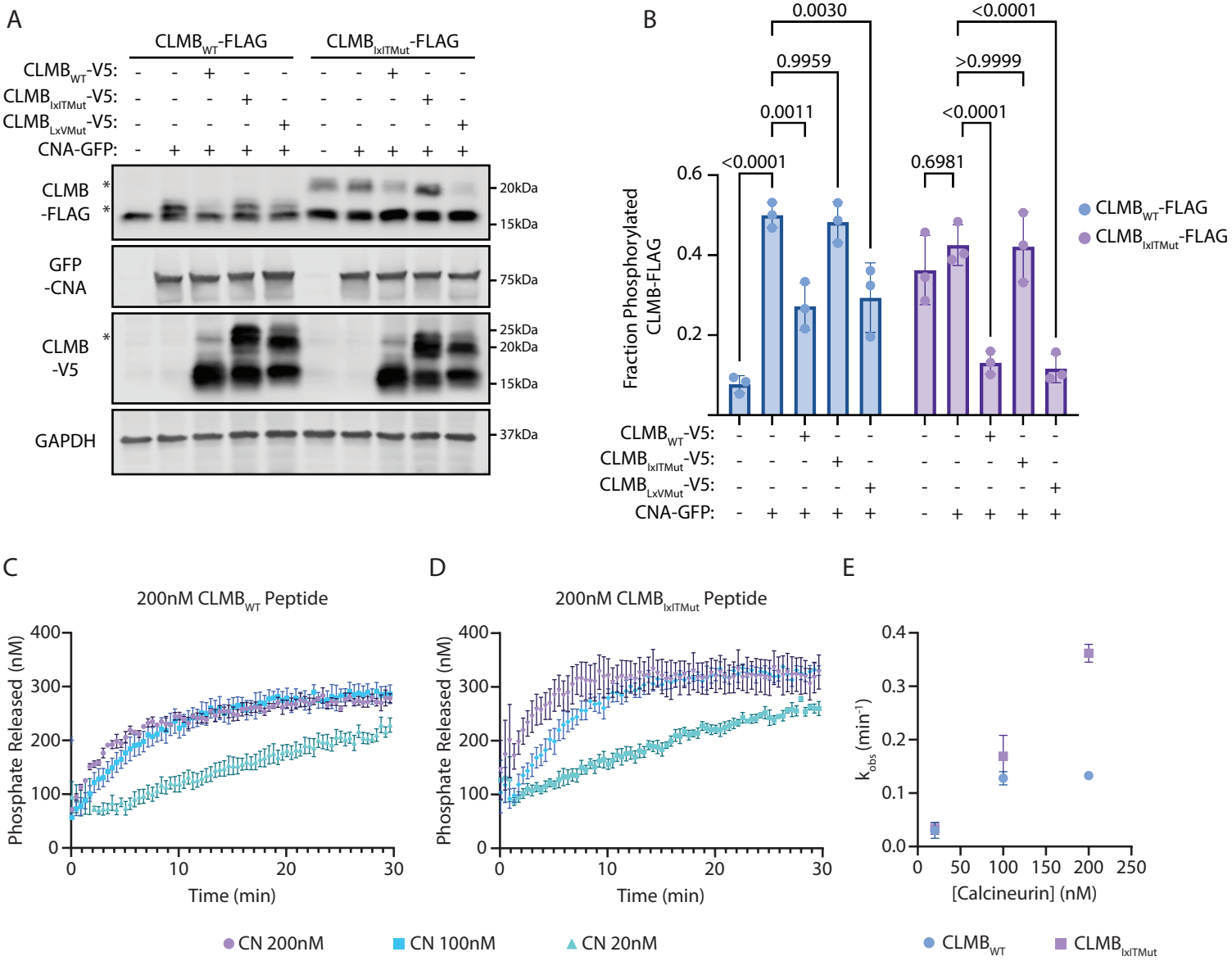
A
CLMB$_{WT}$-FLAG
CLMB$_{IxITMut}$-FLAG
CLMB$_{WT}$-V5:
CLMB$_{IxITMut}$-V5:
CLMB$_{LxVMut}$-V5:
CNA-GFP:
CLMB -FLAG
GFP -CNA
CLMB -V5
GAPDH
20kDa
15kDa
75kDa
25kDa
20kDa
15kDa
37kDa
B
Fraction Phosphorylated CLMB-FLAG
0.0030
<0.0001
0.9959
>0.9999
0.0011
<0.0001
<0.0001
0.6981
CLMB$_{WT}$-FLAG
CLMB$_{IxITMut}$-FLAG
C
200nM CLMB$_{WT}$ Peptide
Phosphate Released (nM)
Time (min)
D
200nM CLMB$_{IxITMut}$ Peptide
Phosphate Released (nM)
Time (min)
CN 200nM
CN 100nM
CN 20nM
E
k_{obs} (min^{-1})
[Calcineurin] (nM)
CLMB$_{WT}$
CLMB$_{IxITMut}$

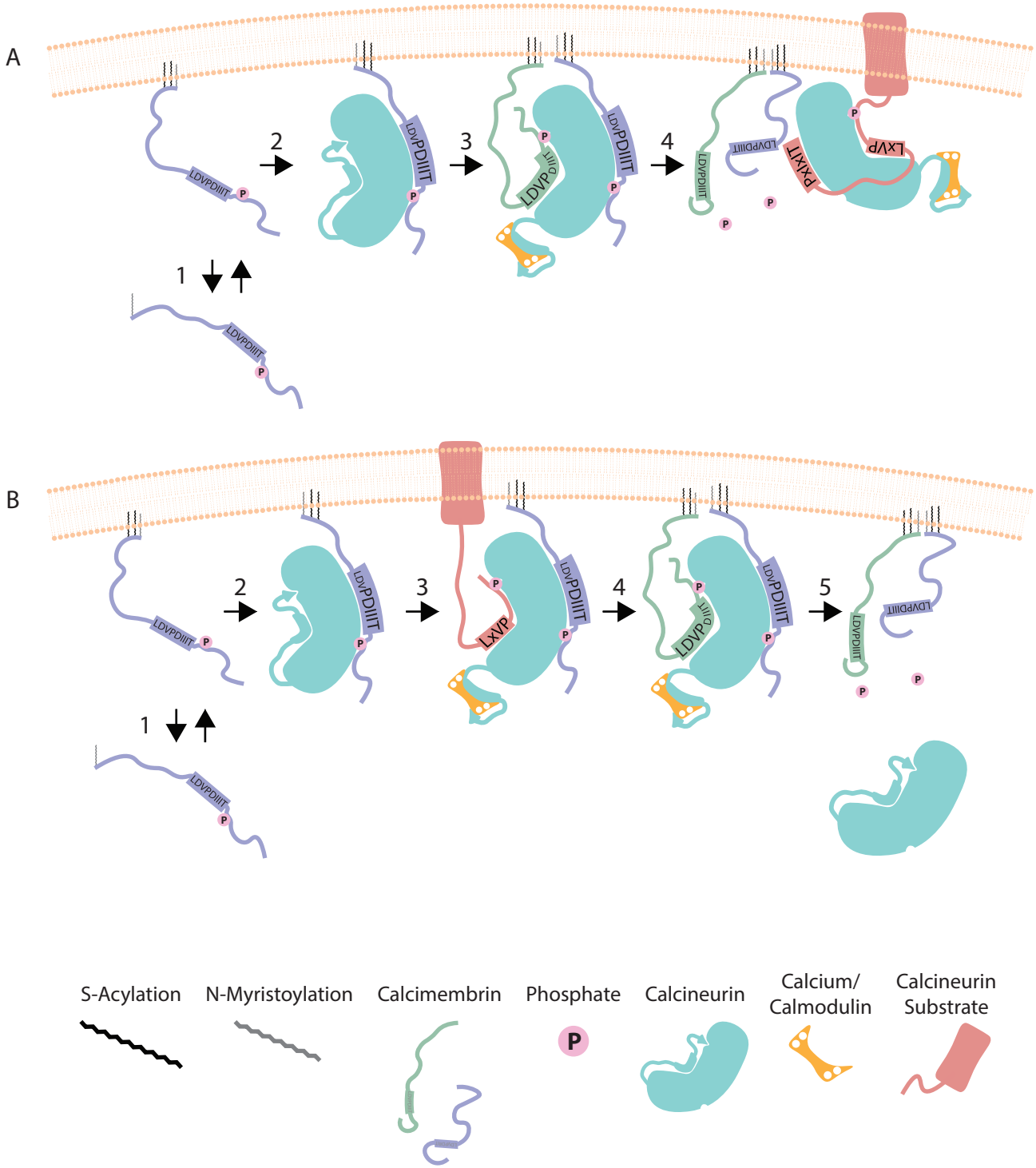
A
B
1
2
3
4
5
LDVPDIIIT
LDVPDIIIT
LDVPDIIIT